Received: 28 October 2020 | Revised: 11 February 2021 | Accepted: 2 March 2021

IET Microwaves, Antennas & Propagation

DOI: 10.1049/mia2.12107

The Institution of Engineering and Technology WILEY

ORIGINAL RESEARCH PAPER

Exact conic section arc elements in 2D and 2.5D FEM using a coordinate transformation

Lorenzo Codecasa[1] | **Gian Guido Gentili**[1] | **Misagh Khosronejad**[1] | **Giuseppe Pelosi**[2] | **Stefano Selleri**[2]

[1]Dipartimento di Elettronica, Informazione e Bioingegneria, Politecnico di Milano, Milano, Italy

[2]Department of Information Engineering, University of Florence, Florence, Italy

Correspondence

Stefano Selleri, Department of information Engineering, University of Florence, Via di S. Marta, 3 I-50139 Florence, Italy.
Email: stefano.selleri@unifi.it

Abstract

This study introduces the conic section arc elements in 2D and 2.5D finite element method (FEM). Elements are obtained by deforming an edge in a standard triangular element through a coordinate transformation. This allows to completely eliminate the geometrical error in structures composed of circular, elliptical, hyperbolic and parabolic arcs. The element order is defined independently of the geometrical description of the boundary, allowing the use of simple meshers. Previously available FEM codes can be straightforwardly modified to introduce the conic section boundaries.

1 | INTRODUCTION

Finite element method (FEM) is nowadays among the most popular numerical techniques for the solution of Maxwell's equations, and its applications comprise guided wave problems and full-wave 3D components and antennas [1, 2]. In the 2D case or 2.5D case [3], the method is based on a 2D mesh which is typically a collection of triangles. Even if a triangular mesh is much more flexible than a rectangular mesh, typical of finite differences [4], due to the straight edges of the mesh, the boundaries of the geometry under analysis are approximated by piecewise straight lines, leading, in some cases, to a significant geometrical error. A fine description of the geometry often requires an exceedingly dense mesh and an unnecessary increase of the degrees of freedom. In common applications, curved lines in the geometry are very often circular or elliptical arcs, for which to the authors' knowledge there is no simple and exact representation in 2D FEM literature. Curved boundaries are usually approximated by isoparametric elements [2, 5, 6] or in the general frame of isogeometric analysis [7, 8]. An exact representation of circles can be obtained by rational B-splines [7, 9, 10], but these require a complex implementation since control points and relative weights must be added and defined outside the element. All these techniques define new discretizations of Maxwell's equations. On the contrary, the method presented here defines an exact transformation of Maxwell's equations into Maxwell's equations themselves with altered permittivity and permeability tensors. Such new equations can be solved numerically with any discretization applicable to a triangular grid, such as FEM, finite integration technique (FIT) [11, 12] or finite volume technique (FV) [13]. More specifically, we define a general transformation that converts straight segments into an arbitrary conic section arcs (circular, elliptical, hyperbolic and parabolic). In a previously developed code, the only modification required is the introduction of an anisotropic material, defined by the transformation, only in the triangles with a curved edge. This ensures that all numerical properties of the technique used are preserved.

A further useful aspect of the proposed technique is the independence of the degree of approximation from the geometrical representation. Although isoparametric elements can provide a good approximation of an arbitrary curved side or surface in 2D and 3D, we believe that the technique we propose can be very useful in practical applications, although limited to 2D and 2.5D, because of three main reasons:

- The independency of the degree of approximation of the field with respect to the geometrical description;
- The possibility to reuse old code with triangular meshes having straight sides and introduce curved edges by a simple change of material properties;

- The possibility to develop new numerical codes, such as FEM, FIT of FV, for triangular meshes with straight edges, since curved edges can be implemented a posteriori with the proposed technique.

All these three aspects represent the main novelty and originality of the proposed technique and are not shared with isoparametric representations. For instance, p-adaptivity can be easily introduced because the geometrical representation is not dependent on the degree of approximation. As compared to the isogeometric approaches, that can exactly represent conic sections [7], an advantage of the proposed technique is the simplicity of the implementation. One can easily implement it in different 2D or 2.5D techniques such as for example [14] by introducing a suitable anisotropic material. Although this study focuses on 2D and 2.5D FEM, the method can potentially be applied also to 3D geometries, a nontrivial extension that is currently under study.

The technique we discuss is limited to the case in which the curved side is a conic section. This is, however, by far the most common case in practice and the usefulness of the technique will be demonstrated by rather a large set of examples in 2D and 2.5D, in particular some critical components such as narrow-band microwave bandpass filters with rounded corners or cylindrical posts, substrate integrated waveguide (SIW) components and a low-pass waffle iron filter with partial height round posts analysed by 2.5D FEM.

The study is organized as follows: in Section 2 we define the coordinate transformation and the corresponding Jacobian. Section 3 is a collection of results: we start with modes computation for circular and elliptical waveguide, then we analyse narrow-band filters in which circular arcs are part of the geometry, then show an application to SIW filters and finally we show an example of application to 2.5D FEM, a waffle iron filter with round teeth. Finally, Section 4 presents some conclusions. Some demonstrations relative to the coordinate transformation are shown in Appendix.

2 | COORDINATE TRANSFORMATIONS

The effect of general coordinate transformations on Maxwell's equations is well known, and their applications have been proposed for example for cloaking [15], antenna pattern manipulation [16] and geometry deformation for efficient analysis of elliptical structures [17, 18], to cite just a few. Often, these approaches are labelled 'transformation optics' [19] or 'transformation electromagnetics' [20]. In our case, coordinate transformations are used to establish an equivalence between the solutions of Maxwell's equation in a meshed geometry with curved triangle edges (in the form of conic section arcs) and a geometry with piecewise straight triangle edges. As it is customary in all cited studies, this happens by introducing in the transformed triangle a suitable anisotropic material.

Let us assume to have a starting, or 'original', system of coordinates (x', y', z') in which one of the edges of the element is a curved arc in plane $x'y'$ and a second, or 'transformed' system of coordinates (x, y, z) in which the triangle has three straight edges in plane xy. Let the transformation then be:

$$x = x(x', y') \tag{1}$$

$$y = y(x', y') \tag{2}$$

$$z = z' \tag{3}$$

with an associated Jacobian (in matrix form)

$$\bar{\mathbf{J}} = \left[\frac{\partial \mathbf{r}}{\partial \mathbf{r}'}\right] = \begin{bmatrix} \frac{\partial x}{\partial x'} & \frac{\partial x}{\partial y'} & 0 \\ \frac{\partial y}{\partial x'} & \frac{\partial y}{\partial y'} & 0 \\ 0 & 0 & 1 \end{bmatrix} = \begin{bmatrix} J_{xx} & J_{xy} & 0 \\ J_{yx} & J_{yy} & 0 \\ 0 & 0 & 1 \end{bmatrix}. \tag{4}$$

A solution of Maxwell's equations $\mathbf{e}'$ and $\mathbf{h}'$ for a given problem in the original coordinate frame x', y', z', with material parameters characterized by tensors $\bar{\boldsymbol{\epsilon}}'$ and $\bar{\boldsymbol{\mu}}'$, is linked to the solution $\mathbf{e}$ and $\mathbf{h}$ in the transformed frame (x, y, z) by:

$$\mathbf{e}' = \bar{\mathbf{J}}^{\mathrm{T}} \cdot \mathbf{e} \tag{5}$$

$$\mathbf{h}' = \bar{\mathbf{J}}^{\mathrm{T}} \cdot \mathbf{h}. \tag{6}$$

providing that the material properties in the transformed frame are set to:

$$\bar{\boldsymbol{\epsilon}}_r = \frac{\bar{\mathbf{J}} \cdot \bar{\boldsymbol{\epsilon}}_r' \cdot \bar{\mathbf{J}}^{\mathrm{T}}}{\det \bar{\mathbf{J}}} \tag{7}$$

$$\bar{\boldsymbol{\mu}}_r = \frac{\bar{\mathbf{J}} \cdot \bar{\boldsymbol{\mu}}_r' \cdot \bar{\mathbf{J}}^{\mathrm{T}}}{\det \bar{\mathbf{J}}}. \tag{8}$$

In order to describe the transformation, we make a constant reference to Figure 1, where the relevant parameters are shown. In the original coordinate system the triangle is defined by points $\mathbf{r}_i'$, $i = 1, 2, 3$ and it has a curved edge, opposite to vertex $\mathbf{r}'_3$. In the transformed coordinate system, the triangle is defined by points $\mathbf{r}_i$, $i = 1, 2, 3$ and all its edges are straight. Moreover, $\mathbf{r}_i' = \mathbf{r}_i$ for every i. We associate to the triangle in the transformed domain a set of barycentric coordinates ζ_i, $i = 1, 2, 3$, such that $\mathbf{r} = \mathbf{r}_1\zeta_1 + \mathbf{r}_2\zeta_2 + \mathbf{r}_3\zeta_3$. The arc between points $\mathbf{r}_1$ and $\mathbf{r}_2$ belongs to a conical section. In the figure $\mathbf{r}_m = \frac{1}{2}(\mathbf{r}_1 + \mathbf{r}_2)$ is the midpoint between $\mathbf{r}_1$ and $\mathbf{r}_2$, $\mathbf{r}_t$ is the intersection of the two lines tangent to the conic section and passing for $\mathbf{r}_1$ and $\mathbf{r}_2$ and $\mathbf{r}_c$ is the intersection between the conic section and the line joining $\mathbf{r}_m$ to $\mathbf{r}_t$.

The inverse transformation that maps continuously points in the triangle with all straight edges to points in the triangle with a curved edge is:

$$\mathbf{r}' = \frac{\mathbf{r} - 2(\mathbf{r}_m - \xi\mathbf{r}_t)\zeta_1\zeta_2}{1 - 2(1-\xi)\zeta_1\zeta_2} \tag{9}$$

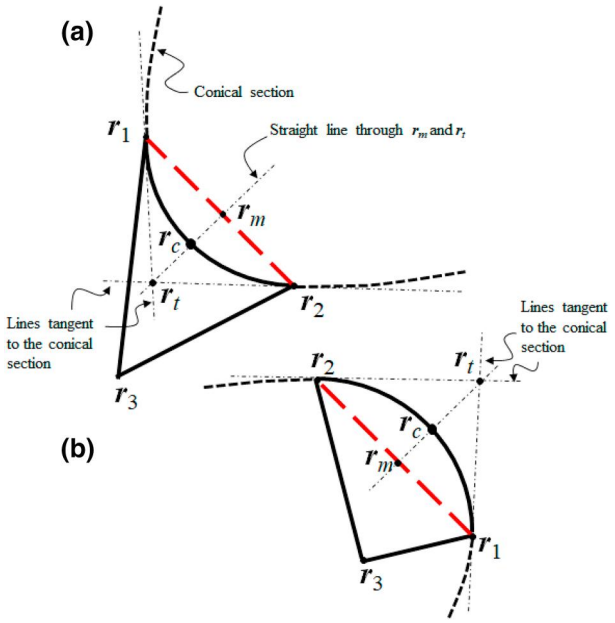

FIGURE 1 Triangles with one curved edge, concave (a) and convex (b), with its mapped parent with straight edges. Relevant geometrical parameters for the two possible cases. $\mathbf{r}_m$ is the midpoint of the edge $\mathbf{r}_1$, $\mathbf{r}_2$. $\mathbf{r}_t$ is the intersection of the two lines tangent to the conic section and passing through $\mathbf{r}_1$ and $\mathbf{r}_2$. $\mathbf{r}_c$ is the intersection of the segment $\mathbf{r}_t$, $\mathbf{r}_m$ with the conic section

in which ξ is a strictly positive parameter identifying point $\mathbf{r}_c$ on the segment $\mathbf{r}_m$, $\mathbf{r}_t$ in the form:

$$\mathbf{r}_c = \frac{1}{1+\xi}\mathbf{r}_m + \frac{\xi}{1+\xi}\mathbf{r}_t. \tag{10}$$

The transformation maps segment $\mathbf{r}_1$, $\mathbf{r}_2$ to a chosen conic section. In order to compute the parameters of the transformation $\mathbf{r}_t$ and ξ we can use the following simple procedure. At first, one should have the conic section defined in an implicit matrix form as:

$$[x' \;\; y' \;\; 1][C]\begin{bmatrix} x' \\ y' \\ 1 \end{bmatrix} = 0 \tag{11}$$

where $[C]$ is a symmetric matrix that contains the coefficients of the polynomial representing the conic section [21].

$$[C] = \begin{bmatrix} c_{xx} & c_{xy}/2 & c_{x1}/2 \\ c_{xy}/2 & c_{yy} & c_{y1}/2 \\ c_{x1}/2 & c_{y1}/2 & c_{11} \end{bmatrix}. \tag{12}$$

Let' us now introduce the compact notation:

$$\langle \mathbf{a}, \mathbf{b} \rangle_C = [a_x \; a_y \; 1][C]\begin{bmatrix} b_x \\ b_y \\ 1 \end{bmatrix}, \qquad \|\mathbf{a}\|_C^2 = \langle \mathbf{a}, \mathbf{a} \rangle_C,$$

defining a pseudo scalar product and a norm[1]. Point $\mathbf{r}_t$ is obtained by solving the following two by two system of linear equations [21]:

$$\langle \mathbf{r}_1, \mathbf{r}_t \rangle_C = 0, \tag{13}$$

$$\langle \mathbf{r}_2, \mathbf{r}_t \rangle_C = 0, \tag{14}$$

Then, finally

$$\xi = \sqrt{\frac{-\frac{1}{2}\langle \mathbf{r}_1, \mathbf{r}_2 \rangle_C}{\|\mathbf{r}_t\|_C^2}}. \tag{15}$$

It can be easily verified that the transformation is the identity along edges $\mathbf{r}_1$, $\mathbf{r}_3$ and $\mathbf{r}_2$, $\mathbf{r}_3$. Note also that two adjacent triangles have the common edge curved in a consistent way. In the Appendix, we show a demonstration of these properties and of the transformation of segment $\mathbf{r}_1$, $\mathbf{r}_2$ to a conic section arc.

We now define the 2×2 matrix $\left[\frac{\partial \mathbf{r}'}{\partial \zeta_i}\right]$. From Equation (9), its elements are given column wise by:

$$\frac{\partial \mathbf{r}'}{\partial \zeta_1} = \frac{\mathbf{r}_1 - \mathbf{r}_3}{d} + 2\zeta_2 \frac{\mathbf{r}(1-\xi) - \mathbf{r}_m + \xi \mathbf{r}_t}{d^2} \tag{16}$$

$$\frac{\partial \mathbf{r}'}{\partial \zeta_2} = \frac{\mathbf{r}_2 - \mathbf{r}_3}{d} + 2\zeta_1 \frac{\mathbf{r}(1-\xi) - \mathbf{r}_m + \xi \mathbf{r}_t}{d^2} \tag{17}$$

where $d = 1 - 2(1-\xi)\zeta_1\zeta_2$. Similarly we define the 2×2 matrix $\left[\frac{\partial \mathbf{r}}{\partial \zeta_i}\right]$ whose elements are given column wise by:

$$\frac{\partial \mathbf{r}}{\partial \zeta_1} = \mathbf{r}_1 - \mathbf{r}_3 \tag{18}$$

$$\frac{\partial \mathbf{r}}{\partial \zeta_2} = \mathbf{r}_2 - \mathbf{r}_3. \tag{19}$$

We have that, letting $\bar{\mathbf{J}}_{tt}$ be the upper 2×2 submatrix of the Jacobian relative to x, y coordinates in Equation (22), that is,

$$\bar{\mathbf{J}}_{tt} = \begin{bmatrix} J_{xx} & J_{xy} \\ J_{yx} & J_{yy} \end{bmatrix} \tag{20}$$

one finds

$$\bar{\mathbf{J}}_{tt}^{-1} = \left[\frac{\partial \mathbf{r}'}{\partial \zeta_i}\right]\left[\frac{\partial \mathbf{r}}{\partial \zeta_i}\right]^{-1} \tag{21}$$

[1]Note that $\|.\|_C^2$ is indefinite, as for example, Minkowski norm [22].

and finally

$$\mathbf{J}_{tt} = \left[\frac{\partial \mathbf{r}}{\partial \zeta_i}\right]\left[\frac{\partial \mathbf{r}'}{\partial \zeta_i}\right]^{-1}. \tag{22}$$

2.1 | Examples for circle and ellipse

For a more straightforward application of the above formulas, we consider two very common cases that can appear in practical applications: the circle and the ellipse.

We first consider a circle centred at $\mathbf{r}_0$ and having a radius R. We have:

$$[C] = \begin{bmatrix} 1/R^2 & 0 & -x_0/R^2 \\ 0 & 1/R^2 & -y_0/R^2 \\ -x_0/R^2 & -y_0/R^2 & x_0^2/R^2 + y_0^2/R^2 - 1 \end{bmatrix} \tag{23}$$

and from Equations (13) and (14), with some simplifications,

$$\begin{bmatrix} x_1 - x_0 & y_1 - y_0 \\ x_2 - x_0 & y_2 - y_0 \end{bmatrix}\begin{bmatrix} x_t \\ y_t \end{bmatrix} = \\ = \begin{bmatrix} (x_1 - x_0)x_0 + (y_1 - y_0)y_0 + R^2 \\ (x_2 - x_0)x_0 + (y_2 - y_0)y_0 + R^2 \end{bmatrix}. \tag{24}$$

Having obtained $\mathbf{r}_t$, one can use Equation (15) to find ξ. Now the parameters of the transformation are completely defined.

A second case, although less common in application, is represented by the ellipse. We limit the expression to an ellipse centred at $\mathbf{r}_0$ with semiaxes a and b along x and y, respectively and no rotation (the case of a rotated ellipse can be easily obtained by introducing the rotation matrix of the rotated coordinate system). For this case we have:

$$[C] = \begin{bmatrix} 1/a^2 & 0 & -x_0/a^2 \\ 0 & 1/b^2 & -y_0/b^2 \\ -x_0/a^2 & -y_0/b^2 & x_0^2/a^2 + y_0^2/b^2 - 1 \end{bmatrix} \tag{25}$$

and from Equations (13) and (14):

$$\begin{bmatrix} (x_1 - x_0)/a^2 & (y_1 - y_0)/b^2 \\ (x_2 - x_0)/a^2 & (y_2 - y_0)/b^2 \end{bmatrix}\begin{bmatrix} x_t \\ y_t \end{bmatrix} = \\ = \begin{bmatrix} (x_1 - x_0)x_0/a^2 + (y_1 - y_0)y_0/b^2 + 1 \\ (x_2 - x_0)x_0/a^2 + (y_2 - y_0)y_0/b^2 + 1 \end{bmatrix}. \tag{26}$$

Also in this case $\mathbf{r}_t$ is computed in closed form and ξ is obtained from Equation (15).

2.2 | Material definition

The implementation in FEM codes is straightforward. For the anisotropic case, one should use Equations (7) and (8) directly with the Jacobian defined by Equation (22). For the common case for which ϵ_r', μ_r' are piecewise uniform scalars, letting $\boldsymbol{\epsilon}_r = \epsilon_r'\boldsymbol{\Lambda}$, $\boldsymbol{\mu}_r = \mu_r'\boldsymbol{\Lambda}$, we have:

$$\boldsymbol{\Lambda} = \frac{1}{\det \mathbf{J}}\begin{bmatrix} J_{xx}^2 + J_{xy}^2 & J_{xx}J_{yx} + J_{yy}J_{xy} & 0 \\ J_{xx}J_{yx} + J_{yy}J_{xy} & J_{yy}^2 + J_{yx}^2 & 0 \\ 0 & 0 & 1 \end{bmatrix} \tag{27}$$

where $\det \mathbf{J} = J_{xx}J_{yy} - J_{xy}J_{yx}$. Letting finally,

$$\boldsymbol{\Lambda} = \begin{bmatrix} \Lambda_{xx} & \Lambda_{xy} & 0 \\ \Lambda_{yx} & \Lambda_{yy} & 0 \\ 0 & 0 & \Lambda_{zz} \end{bmatrix} \tag{28}$$

one gets

$$\boldsymbol{\Lambda}^{-1} = \begin{bmatrix} \Lambda_{yy} & -\Lambda_{xy} & 0 \\ -\Lambda_{yx} & \Lambda_{xx} & 0 \\ 0 & 0 & \Lambda_{zz}^{-1} \end{bmatrix}. \tag{29}$$

It is noted that the transformation only affects the triangles for which one edge is curved, leaving the rest of the mesh (and of the material) unaltered. The implementation is simple, since 2D meshers usually provide circular arc segments information such as radius and centre location or elliptical arcs defined by semiaxes, centre location and rotation (see e.g. Matlab pdetoolbox™). Existing simple triangular meshes solving a specific problem can be adapted to the implementation of curved elements by a simple modification of the material and the use of numerical quadrature over triangles. Some results are presented in the next section showing the excellent performance of the elements in the analysis of some critical components in 2D, such as the narrow band H-plane filters and in 2.5D [3], a low-pass filter with rounded partial-height posts.

3 | RESULTS

As a first example, we show the results obtained in the computation by FEM of circular waveguide modes and elliptical waveguide modes. We first note that since the coordinate transformation is in xy plane only, no z component of the field is produced by Equations (5) and (6), so transverse electric modes (TE modes) are still TE and transverse magnetic modes (TM modes) are still TM. The waveguides, together with the meshes used, are shown in Figure 2. Details of the weak form solved by FEM can be found in several books [1]. Table 1 shows results attained via second-order scalar elements with the technique proposed and with standard isoparametric

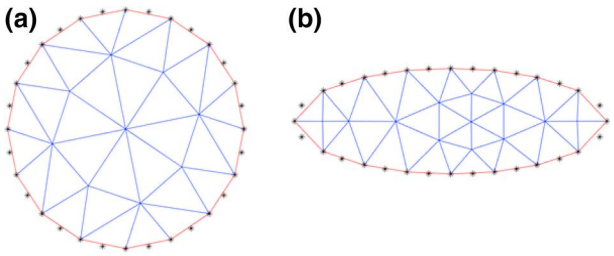

FIGURE 2 Circular waveguide of unit radius and mesh used to compute the modes in Table 1, elliptical waveguide of axial ratio 3 and mesh used to compute the modes in Table 2. Points used for isoparametric mapping are shown too as asterisks

TABLE 1 Normalized wavenumber for the first five TE and TM modes obtained with the mesh in Figure 2a. Circular waveguide of the unit radius

TE exact	Isoparametric (error)	This work (error)
1.8412	1.8418 (0.0308%)	1.8417 (0.0282%)
1.8412	1.8418 (0.0308%)	1.8417 (0.0282%)
3.0542	3.0617 (0.2431%)	3.0616 (0.2416%)
3.0542	3.0625 (0.2721%)	3.0624 (0.2683%)
3.8317	3.8532 (0.5619%)	3.8531 (0.5579%)
TM exact	**Isoparametric (error)**	**This work (error)**
2.4048	2.4064 (0.0662%)	2.4064 (0.0638%)
3.8317	3.8447 (0.3380%)	3.8445 (0.3343%)
3.8317	3.8447 (0.3380%)	3.8445 (0.3343%)
5.1356	5.2148 (1.5416%)	5.2145 (1.5363%)
5.1356	5.2430 (2.0908%)	5.2433 (2.0967%)

Note: Comparison between exact results, isoparametric elements of degree 2 and exact circular arcs.

elements for the waveguide in Figure 2a. Error is computed w.r.t. the analytical solution. Integrals relative to the anisotropic material are computed by standard quadrature over triangles. The comparison in Table 1 shows the effect of geometrical error for a rather coarse mesh. As the mesh density increases, the performance of isoparametric elements tends to coincide with that of the technique discussed. Similar behaviour is found for the elliptical waveguide in Figure 2b. The results obtained with isoparametric elements and with our technique are shown in Table 2. Also in this case there is small difference in the performance, enlightening the effect of geometrical error.

An analysis relative to the effect of numerical integration is shown in Figure 3. We computed the error in the wavenumber of the first three TE modes as a function of the number of quadrature points in the triangle. The figure clearly shows that the quadrature rule has no effect on the final result providing it is not too low. The rule used corresponds to 7 points for rule 5 and 48 points for rule 15.

The second example is shown in Figure 4, in which a metallic full-height post is placed in a WR75 rectangular

TABLE 2 Normalized wavenumber for the first five TE and TM modes obtained with the mesh in Figure 2b

TE exact	Isoparametric (error)	This work (error)
1.8805	1.8811 (0.0302%)	1.8808 (0.0154%)
3.4572	3.4595 (0.0647%)	3.4589 (0.0476%)
5.0100	5.0179 (0.1577%)	5.0170 (0.1415%)
5.1497	5.1557 (0.1183%)	5.1556 (0.1164%)
6.2316	6.2491 (0.2797%)	6.2489 (0.2766%)
TM exact	**Isoparametric (error)**	**This work (error)**
5.2890	5.2969 (0.1509%)	5.2967 (0.1454%)
6.4308	6.4501 (0.2996%)	6.4498 (0.2944%)
7.6540	7.6929 (0.5084%)	7.6926 (0.5044%)
8.9408	9.0228 (0.9180%)	9.0227 (0.9167%)
9.9637	10.0617 (0.9834%)	10.0610 (0.9760%)

Note: Elliptical waveguide of axial ratio 3. Comparison between exact results, isoparametric elements of degree 2 and exact elliptical arcs. Eigenvalues are computed for a major semiaxis of length 1.

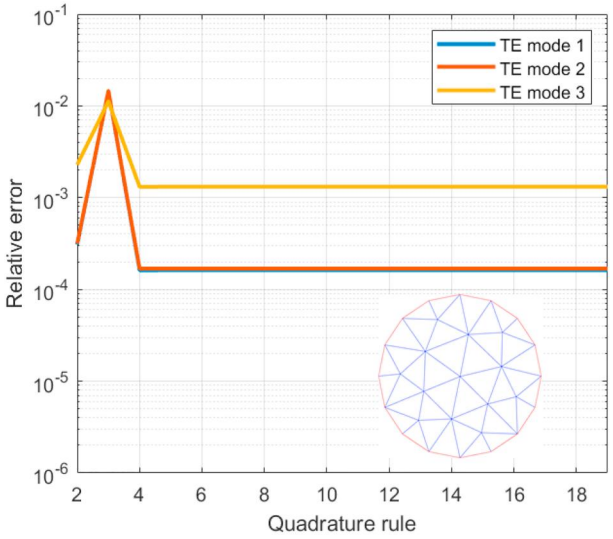

FIGURE 3 Relative error in the computation of the wavenumber of the first three TE modes for curved edges. When the quadrature rule is larger than four (corresponding to six points) the results are no longer dependent on the rule

waveguide [23]. The analysis has been carried out using first-order edge elements and the magnetic field formulation of FEM [3]. The figure shows the convergence of parameter $|S_{11}|$ in dB ($20\log_{10}|S_{11}|$) at 13 GHz by varying the number of segments approximating the circular post. The number of segments is the result of mesh refinement or mesh generation with some maximum edge size, therefore when the number of segments is increased a denser mesh is consequently generated. The figure represents therefore the combined effect of mesh refinement and geometrical approximation. It is clear that the exact geometrical representation is a drastic accuracy improvement. Even when a rather large number of segments

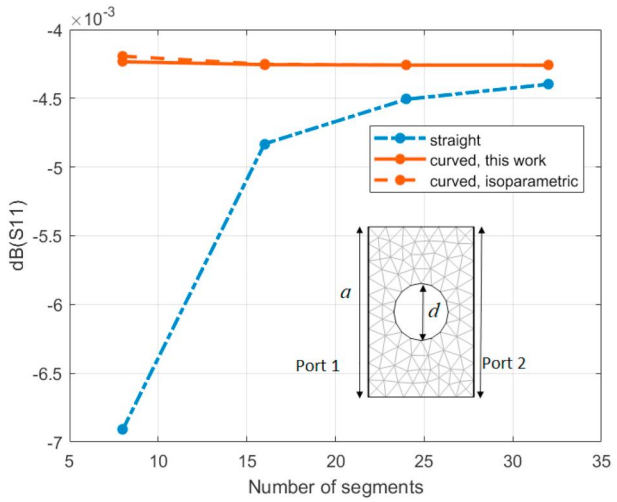

FIGURE 4 Metallic post in WR75 rectangular waveguide, $a = 19.05$ mm, $d = 6.4$ mm. Convergence of $|S_{11}|$ as a function of the number of segments used to describe the circular post

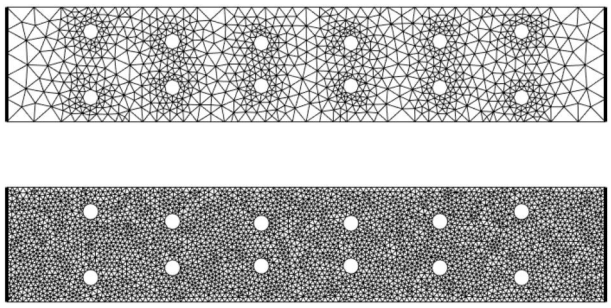

FIGURE 5 Two meshes used for the analysis of the filter in [24]

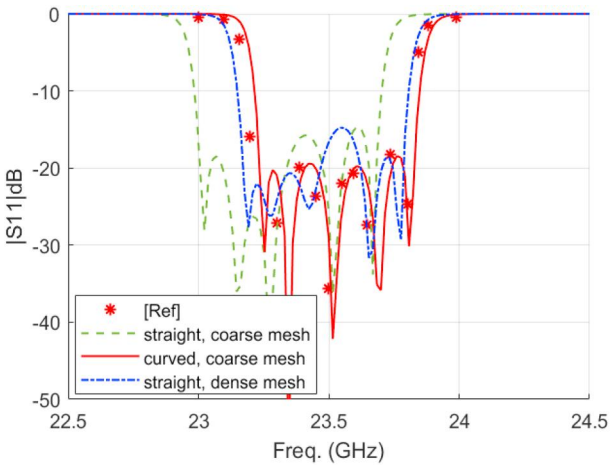

FIGURE 6 Filter with full-height metallic round posts designed in [24]. Comparison between curved elements and straight elements. The meshes used for the analysis are shown in Figure 5

are used to represent the circle, there is still a rather significant impact on the computed S-parameters. The analysis clearly shows that a very dense mesh is not necessary, since it only acts in the sense of decreasing the geometrical error. When critical components are analysed, such as narrow-band waveguide filters, the impact of the geometrical error in the final frequency response is not negligible, as it is shown in the next examples. The figure also shows the very small difference in the computed S-parameters between exact circular arcs and the corresponding isoparametric approximation. The difference shown tends to vanish quickly as the number of segments to describe the circle increases. This aspect should be taken into account in view of potential applications: isoparametric elements behave very well when the mesh is not coarse, so one should not expect significantly different performances using the proposed technique. But the possibility to use an arbitrary degree of approximation for the field with no change in the mesh definition seems attractive and leads to a simple implementation in numerical FEM codes.

Starting from the previous result, the impact of exact geometrical description on a narrow-band filter with symmetrically placed full-height circular metallic posts is considered. In order to better appreciate the effect of an accurate geometrical description of the posts, we used two meshes for the analysis, a coarse mesh and a dense mesh, shown in Figure 5. The coarse mesh is composed of 1783 triangles and the dense mesh of 7418 triangles. The S-parameters have been computed for the coarse mesh case with straight and curved edges and for the dense mesh with straight edges. Vector elements of second order have been used in the analysis. The results are shown in Figure 6, together with reference data in [24] computed with a different method based on equivalent sources. The use of circular arc elements greatly improves the agreement with [24] and represents a large speed up factor. For comparison, the analysis with the coarse mesh took only 0.25 s/freq (using straight or curved edges), whereas the analysis with the dense mesh and straight edges took 1.2 s/freq. Note that the use of a denser mesh improves the agreement with reference data as expected, but not as much as what obtained by curved edges in the coarse mesh, especially in the level of reflection coefficient. Curved edges represent therefore a major improvement for the very little cost of filling up the matrix with a suitable material. Results obtained with the isoparametric elements overlap with those obtained by the proposed technique and are not shown in the figure.

A further example is shown in Figure 7, in which a four-cavity filter has been realized using symmetrical irises with rounded edges as a result of milling a mould [25] (an iris is shown in the inset for clarity). Also in this case, accurate results are obtained with a rather coarse mesh (shown in the figure) thanks to the exact representation of the geometry obtained by circular arc elements. Again, the use of standard triangles, as those plotted in the inset of the figure (labelled 'straight edges'), leads to significant loss of accuracy.

Results for a filter with full-height dielectric posts are shown in Figure 8. The filter has been analysed with FEM using standard triangles (straight edges) and curved triangles and both curves are compared with the results in [26] obtained by an accurate hybrid mode-matching. Also in this case, the introduction of an exact representation of the geometry

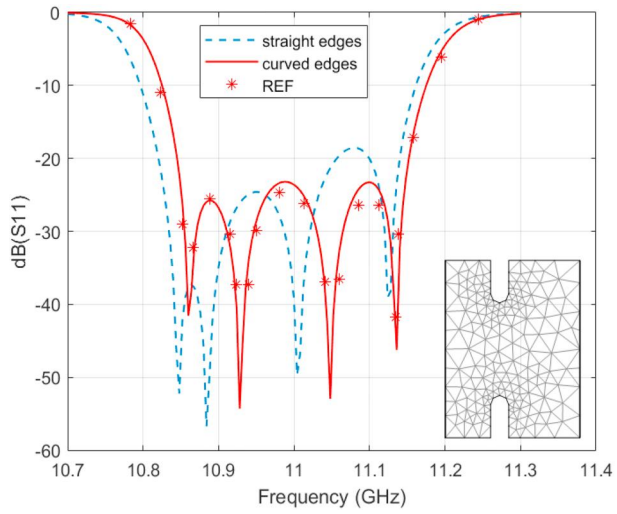

FIGURE 7 Filter with symmetrical irises with round edges designed in [25]. Comparison between curved .elements and straight elements. A detail of the mesh used for the analysis is shown

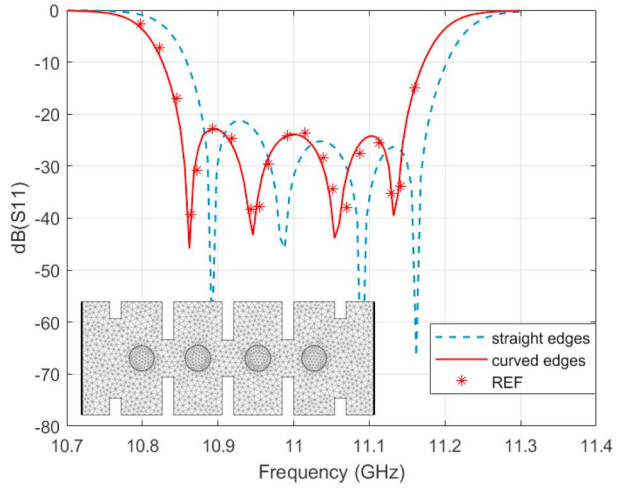

FIGURE 8 Filter with full-height dielectric round posts designed in [26]. Comparison between curved elements edges and straight elements edges. The mesh used for the analysis is shown

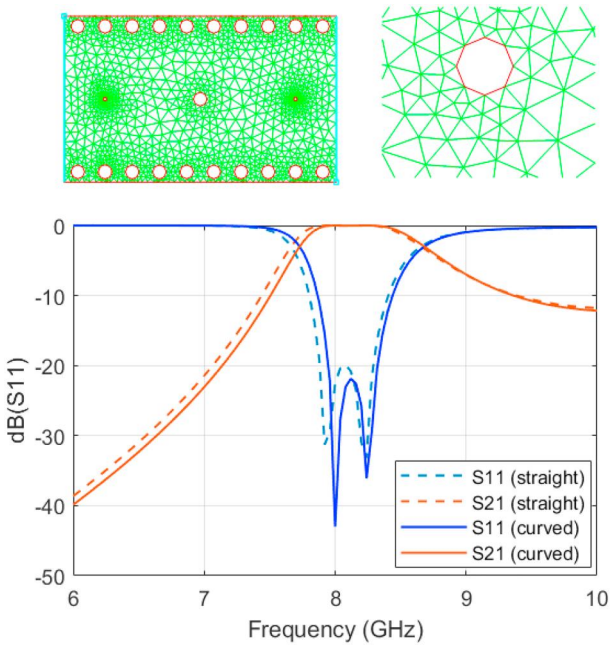

FIGURE 9 Filter in the SIW technology analysed in [27] by BI-RME. In the inset of the figure the mesh used is shown, together with a closeup of the mesh in proximity of the thin input and output centred posts

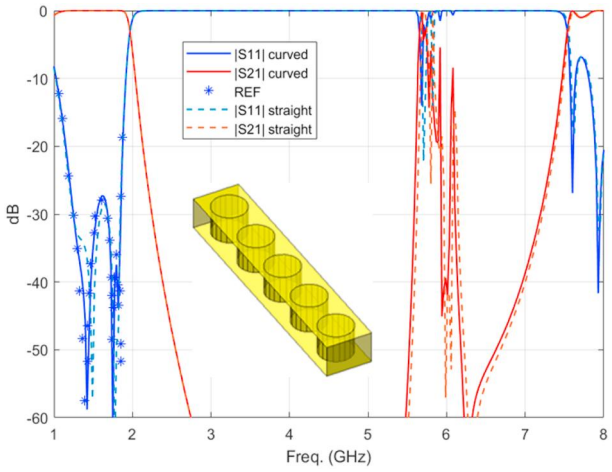

FIGURE 10 Waffle iron filter proposed in [28]. A section of partial height circular posts is shown in the figure. Effect of exact geometrical representation

improves considerably the agreement with the reference results. In this case, both convex and concave curvature elements are present and the continuity of the transformation across different triangles is exploited. Also in this case, the analysis with isoparametric elements does not lead to significant differences in the computed S-parameters.

An application for which exact geometrical representation of circular arcs is very important is the SIW technology, because small radius circular posts are often used both to build cheaply the rectangular waveguide walls and to introduce scattering elements in the device topology. As an example, a two-resonator filter in SIW has been designed and analysed by BI-RME in [27]. The same filter has been analysed and the results are shown in Figure 9. The figure depicts the mesh used in the analysis, together with a closeup in proximity of the thin inner input and output posts. Note that the circle is represented by eight segments (which is the minimum number of segments in Matlab mesher) and this allows to keep the mesh density to a very reasonable size. For this case, the effect of the curvature of the posts is clearly seen in the S-parameters shown in Figure 9. Despite the simple structure, we can observe the usual right shift and a small change in the S_{11} level. These effects are mainly due to the central posts, whereas the lateral posts representing the SIW waveguide have a negligible effect on the scattering parameters. Thanks to the use of curved elements, the analysis took only 0.2 s/freq.

Finally, the technique proposed was used also in the frame of 2.5D FEM [3]. The effect of curved boundaries was tested for the waffle-iron filter proposed in [28] and analysed in [3] by 2.5D FEM. The results are shown in Figure 10. Also in this case, the benefit of curved elements in the S-parameters computation is clearly seen in the plotted curves. A closer agreement with reference data is found in the passband and a small frequency shift is observed with respect to the case of straight segments.

4 | CONCLUSIONS

A simple technique to implement conic section arc elements in 2D FEM and 2.5D FEM has been introduced by the use of a coordinate transformation. A suitable artificial anisotropic material represents in an equivalent form the conic section arc in the mesh. The implementation therefore only requires a modification of the FEM matrix filling, since, unlike isoparametric elements, the element order is completely independent of the geometrical shape. Several examples demonstrate the benefits of exact geometrical representation in critical components such as the passband and low-pass filters using circular posts or rounded corners. The proposed approach can represent a simple and powerful alternative to introduce curved elements, although presently limited to the case of 2D triangular meshes.

ORCID

Lorenzo Codecasa https://orcid.org/0000-0002-2851-3698
Gian Guido Gentili https://orcid.org/0000-0001-9533-8458
Misagh Khosronejad https://orcid.org/0000-0002-4161-1284
Giuseppe Pelosi https://orcid.org/0000-0002-6826-0955
Stefano Selleri https://orcid.org/0000-0003-3090-1451

REFERENCES

1. Pelosi, G., Coccioli, R., Selleri, S.: Quick Finite Elements for Electromagnetic Waves, 2nd edn. Artech House, Boston, MA (2009)
2. Jin, J.: The Finite Element Method in Electromagnetics, 2nd edn. John Wiley and Sons, New York (2002)
3. Gentili, G.G., Accatino, L., Bertin, G.: The generalized 2.5-D finite-element method for analysis of waveguide components. IEEE Trans. Microw. Theor. Tech. 64(8), 2392–2400 (2016)
4. Taflove, A., Hagness, S.C.: Computational Electrodynamics: The Finite-Difference Time-Domain Method. Artech House, Boston, MA (2005)
5. Graglia, R.D., Wilton, D.R., Peterson, A.F.: Higher order interpolatory vector bases for computational electromagnetics. IEEE Trans. Antenn. Propag. 45(3), 329–342 (1997)
6. Pasquetti, R.: Comparison of some isoparametric mappings for curved triangular spectral elements. J. Comput. Phys. 316, 573–577 (2016)
7. Hughes, T.J.R., Cottrell, J.A., Bazilevs, Y.: Isogeometric analysis: CAD, finite elements, NURBS, exact geometry and mesh refinement. Comput. Methods Appl. Mech. Eng. 194(39–41), 4135–4195 (2005)
8. Vázquez, R., et al.: Isogeometric finite elements with surface impedance boundary conditions. IEEE Trans. Magn. 50(2), 429–432 (2014)
9. Martini, E., Pelosi, G., Selleri, S.: A hybrid finite-element-modal-expansion method with a new type of curvilinear mapping for the analysis of microwave passive devices. IEEE Trans. Microw. Theor. Tech. 51(6), 1712–1717 (2003)
10. Martini, E., Selleri, S.: Innovative class of curvilinear tetrahedral elements. Electron Lett. 37(9), 557–558 (2001)
11. Codecasa, L., Trevisan, F.: Constitutive equations for discrete electromagnetic problems over polyhedral grids. J. Comput. Phys. 225(2). 1894–1918 (2007)
12. Codecasa, L., Politi, M.: Explicit, consistent, and conditionally stable extension of FD-TD to tetrahedral grids by FIT. IEEE Trans. Magn. 44(6), 1258–1261 (2008)
13. Yang, M., Chen, Y., Raj, M.: Hybrid finite-difference/finite-volume time-domain analysis for microwave integrated circuits with curved PEC surfaces using a nonuniform rectangular grid. IEEE Trans. Microw. Theor. Techn. 48(6), 969–975 (2000)
14. Kapidani, B., Codecasa, L., Schöberl, J.: An arbitrary-order cell method with block-diagonal mass-matrices for the time-dependent 2D Maxwell equations. J. Comput. Phys. 433, (2021)
15. Keivaan, A., et al.: Design of coating materials for cloaking and directivity enhancement of cylindrical antennas using transformation optics. IEEE Antenn. Wireless Propag. Lett. 16, 3122–3125 (2017)
16. Mitchell-Thomas, R.C., Ebrahimpouri, M., Quevedo-Teruel, O.: Altering antenna radiation properties with transformation optics. 2015 9th European conference on antennas and propagation. EuCAP, Lisbon, pp. 1–2 (2015)
17. Gentili, G.G., et al.: An efficient 2.5-D finite-element approach based on transformation optics for the analysis of elliptical horns. IEEE Trans. Antenn. Propag. 66(9), 4782–4790 (2018)
18. Gentili, G.G., et al.: Analysis of elliptical structures with constant axial ratio by 2.5D finite element method and transformation optics. European microwave conference, Madrid, pp. 1–4 (2018)
19. Pendry, J.B., Schurig, D., Smith, D.R.: Controlling electromagnetic electromagnetic fields. Science. 312(5514), 1780–1782 (2006)
20. Kwon, D.H., Werner, D.H.: Transformation electromagnetics: an overview of the theory and applications. IEEE Antenn. Propag. Mag. 52(1), 24–46 (2010)
21. Downs, J.W.: Practical Conic Sections. Dale Seymour, Palo Alto (1993)
22. Sard, R.D.: Relativistic Mechanics - Special Relativity and Classical Particle Dynamics. W. A. Benjamin, New York (1970)
23. Gentili, G.G., et al.: Circular arc elements in 2D FEM using transformation optics. In: 2019 IEEE MTT-S international conference on numerical electromagnetic and multiphysics modelling and optimization. (NEMO), Boston, pp. 1–3 (2019)
24. Meyer, P.: The design and analysis of waveguide E-plane filters with multiple round inductive posts using a moment-method approach. In: Proceedings of IEEE. AFRICON. Stellenbosch. 1, 532–535 (1996)
25. Belenguer, A., et al.: Efficient modal analysis of arbitrarily shaped H-plane two-port waveguide devices using the 2D parallel-plate Green's function. IET Microw., Antennas Propag. 3(1), 62–70 (2009)
26. Bachiller, C., et al.: Hybrid mode matching method for the efficient analysis of metal and dielectric rods in H plane rectangular waveguide devices. IEEE Trans. Microw. Theor. Techn. 58(12), 3634–3644 (2010)
27. Bozzi, M., Perregrini, L., Ke Wu, K.: Modelling of conductor, dielectric, and radiation losses in substrate integrated waveguide by the boundary integral-resonant mode expansion method. IEEE Trans. Microw. Theor. Techn. 56(12), 3153–3161 (2008)
28. Bunger, R., Arndt, F.: Moment-method analysis of arbitrary 3-D metallic N-port waveguide structures. IEEE Trans. Microw. Theor. Techn. 48(4), 531–537 (2000)

How to cite this article: Codecasa L, Gentili GG, Khosronejad M, Pelosi G, Selleri S. Exact conic section arc elements in 2D and 2.5D FEM using a coordinate transformation. *IET Microw. Antennas Propag.* 2021;1–9. https://doi.org/10.1049/mia2.12107

APPENDIX

We now demonstrate that the transformation Equation (9) maps the segment $\mathbf{r}_1, \mathbf{r}_2$ to the conic section arc in Figure 1 if parameter ξ is chosen according to Equation (15). At first, we demonstrate that point $\mathbf{r}_c$ is on the conic section if Equation (15) holds.

A.1 | Demonstration of (15)

The conic section is defined by:

$$\|\mathbf{r}'\|_C^2 = 0. \tag{30}$$

Since $\mathbf{r}_c$ belongs to the conic:

$$\|\mathbf{r}_c\|_C^2 = 0 \tag{31}$$

from which, recalling Equation (10):

$$\frac{1}{(1+\xi)^2}\,\|\mathbf{r}_m\|_C^2 + \frac{\xi}{(1+\xi)^2}\,\langle \mathbf{r}_m, \mathbf{r}_t\rangle_C + \frac{\xi^2}{(1+\xi)^2}\,\|\mathbf{r}_t\|_C^2 + \frac{\xi}{(1+\xi)^2}\,\langle \mathbf{r}_t, \mathbf{r}_m\rangle_C = 0.$$

Thus, since $\mathbf{r}_m = \frac{1}{2}(\mathbf{r}_1 + \mathbf{r}_2)$, recalling Equations (13) and (14), it follows:

$$\|\mathbf{r}_m\|_C^2 + \xi^2\,\|\mathbf{r}_t\|_C^2 = 0. \tag{32}$$

Also, since $\mathbf{r}_1$ and $\mathbf{r}_2$ are on the conic section, $\|\mathbf{r}_1\|_C^2 = \|\mathbf{r}_2\|_C^2 = 0$, so that:

$$\|\mathbf{r}_m\|_C^2 = \frac{1}{2}\langle \mathbf{r}_1, \mathbf{r}_2\rangle$$

and

$$\xi^2 = -\frac{1}{2}\,\frac{\langle \mathbf{r}_1, \mathbf{r}_2\rangle_C}{\|\mathbf{r}_t\|_C^2}.$$

A.2 | Demonstration of the mapping from a straight segment to a conic section arc

Let's consider a generic point on the segment $\mathbf{r}_1$, $\mathbf{r}_2$, so that $\mathbf{r} = \mathbf{r}_1\zeta_1 + \mathbf{r}_2\zeta_2$ with $\zeta_1 = 1 - \zeta_2$. We now demonstrate that $\mathbf{r}'$, defined by Equation (9), is on the conic section arc, that is $\|\mathbf{r}'\|_C^2 = 0$. From Equation (9) we have:

$$d^2\|\mathbf{r}'\|_C^2 = \|\mathbf{r}_1(1-\zeta_2) + \mathbf{r}_2\zeta_2 - 2(1-\zeta_2)\zeta_2(\mathbf{r}_m - \xi\mathbf{r}_t)\|_C^2 \tag{33}$$

where $d = 1 - 2(1-\zeta_2)\zeta_2(1-\xi)$ is not 0. The right hand term of Equation (33) can be rewritten as:

$$\begin{aligned}
&\|\mathbf{r}_1(1-\zeta_2) + \mathbf{r}_2\zeta_2 - 2(1-\zeta_2)\zeta_2(\mathbf{r}_m - \xi\mathbf{r}_t)\|_C^2 \\
&= \left\|\mathbf{r}_1(1-\zeta_2)^2 + \mathbf{r}_2\zeta_2^2 + 2(1-\zeta_2)\zeta_2\xi\mathbf{r}_t\right\|_C^2 \\
&= 2\zeta_2^2(1-\zeta_2)^2\langle \mathbf{r}_1, \mathbf{r}_2\rangle_C + 4\zeta_2^2(1-\zeta_2)^2\xi^2\|\mathbf{r}_t\|_C^2 \\
&= 4\zeta_2(1-\zeta_2)^2\left(\frac{1}{2}\langle \mathbf{r}_1, \mathbf{r}_2\rangle_C + \xi^2\|\mathbf{r}_t\|_C^2\right)
\end{aligned}$$

and since from Equation (15):

$$\xi^2 = -\frac{1}{2}\,\frac{\langle \mathbf{r}_1, \mathbf{r}_2\rangle_C}{\|\mathbf{r}_t\|_C^2}$$

it follows from Equation (33)

$$d^2\|\mathbf{r}'\|_C^2 = 0$$

and therefore $\|\mathbf{r}'\|_C^2 = 0$.

A.3 | Demonstration of continuity across triangles

It is easy to demonstrate continuity across triangles. At first we show that for edges $\mathbf{r}_1$, $\mathbf{r}_3$ and $\mathbf{r}_2$, $\mathbf{r}_3$ the transformation Equation (9) is the identity. Since for those edges, we have either $\zeta_1 = 0$ or $\zeta_2 = 0$, we have by substitution $\mathbf{r}' = \mathbf{r}$.

Considering a curved common edge between two adjacent triangles, since for both triangles $\mathbf{r}_m$, $\mathbf{r}_t$ and $\mathbf{r}_c$ are the same, a point belonging to the straight common edge is mapped to the same point on the common curved edge by the transformation of each triangle, since such a transformation depends only on the simplex coordinates $\zeta_1 = 1 - \zeta_2$ and ζ_2 which are consistent across the common edge for both triangles. The transformation is therefore continuous also across triangles sharing a common curved edge.